

Uniformity of Drug Payload and Its Effect on Stability of Solid Lipid Nanoparticles Containing an Ester Prodrug

Jin-Ki Kim,[†] Melissa D. Howard,[‡] Thomas D. Dziubla,[§] John J. Rinehart,[‡] Michael Jay,^{†,||} and Xiuling Lu^{*,†}

[†]Division of Molecular Pharmaceutics, Center for Nanotechnology in Drug Delivery, Eshelman School of Pharmacy and Lineberger Comprehensive Cancer Center, University of North Carolina at Chapel Hill, Chapel Hill, North Carolina, United States, [‡]Department of Pharmaceutical Sciences, College of Pharmacy, University of Kentucky, Lexington, Kentucky, United States, [§]Department of Chemical and Materials Engineering, University of Kentucky, Lexington, Kentucky, United States,

^{||}Department of Medicine, University of Kentucky, Lexington, Kentucky, United States, and ^{||}Joint Department of Biomedical Engineering, University of North Carolina at Chapel Hill/North Carolina State University, Chapel Hill, North Carolina, United States

Nanocarriers have been largely investigated to improve the therapeutic efficacy and reduce the toxicity of cancer chemotherapeutic agents for treatment of solid tumors.^{1–3} The unique nanoscale features and innovative designs of nanocarriers can enhance the selectivity of drug delivery to specific tissues.⁴ Although much effort has been directed to deliver drugs specifically to tumors, achieving long circulation times of the nanocarriers and effective delivery of drugs to tumor cells remains a challenge.^{5,6} Thorough characterization of nanocarriers and adequate prediction of their behavior in a biological environment are essential for future clinical application of nanotechnology-based cancer therapy.⁷ Commonly, drug molecules are assumed to be homogenously distributed in nanocarriers, and nanocarrier suspensions are considered as a uniform collection of particles.^{7,8} In fact, a nanocarrier system may consist of populations that have different compositions, sizes, and surface properties. The fate of individual nanoparticles *in vivo* might be different among these nanocarrier populations due to this nonuniformity. Content uniformity and batch-to-batch reproducibility are critical factors considered during the regulatory approval process of nanocarrier systems and are key parameters of the assay cascade performed by the National Cancer Institute's Nanotechnology Characterization Laboratory for novel nanoparticle-based drug delivery systems. In order to achieve a reliable prediction of their effectiveness *in*

ABSTRACT Nanocarrier systems are frequently characterized by their size distribution, while drug encapsulation in nanocarriers is generally characterized in terms of an entire population, assuming that drug distribution is uniform. Careful characterization of nanocarriers and assessment of their behavior in biological environments are essential for adequate prediction of the fate of the nanoparticles *in vivo*. Solid lipid nanoparticles containing [³H]-dexamethasone palmitate (an ester prodrug) and [¹⁴C]-stearyl alcohol (a component of the nanoparticle matrix) were prepared using the nanotemplate engineering method for bioresponsive tumor delivery to overcome interstitial fluid pressure gradients, a physiological barrier to tumor uptake of chemotherapeutic agents. While particle size analysis indicated a uniform size distribution of 93.2 ± 0.5 nm, gel filtration chromatography (GFC) revealed two nanoparticle populations. Drug encapsulation efficiency was 97%, but it distributed differently in the two populations, with average drug/lipid ratios of 0.04 and 0.25, respectively. The difference in surface properties resulted in distinguishing protein adsorption features of the two populations. GFC and HPLC profiles of the mixture of nanoparticles and human serum albumin (HSA) showed that no HSA was adsorbed to the first population of nanoparticles, but minor amounts were adsorbed to the second population. After 24 h incubation in 50% human plasma, $\geq 80\%$ of the [³H]-dexamethasone palmitate was associated with nanoparticles. Thus, characterization of solid lipid nanoparticles produced by this method may be challenging from a regulatory perspective, but the strong association of the drug with the nanoparticles in plasma indicates that this nanocarrier system has the potential for *in vivo* application.

KEYWORDS: nanoparticle · dexamethasone · encapsulation · stability · gel filtration chromatography

vivo, a precise characterization of nanocarriers *in vitro* is necessary. In addition, the drug biodistribution is dependent on the stability of the association of drug molecules with nanocarriers under physiological conditions.

We previously described a solid lipid nanoparticle (NP) containing dexamethasone (DEX) as an adjuvant to reduce the interstitial fluid pressure (IFP) of solid tumors and enhance the tumor uptake of chemotherapeutic agents.^{9,10} By administering a nanomedicine containing the widely used

*Address correspondence to xiuling.lu@unc.edu.

Received for review September 9, 2010 and accepted December 07, 2010.

Published online December 15, 2010. 10.1021/nn102357y

© 2011 American Chemical Society

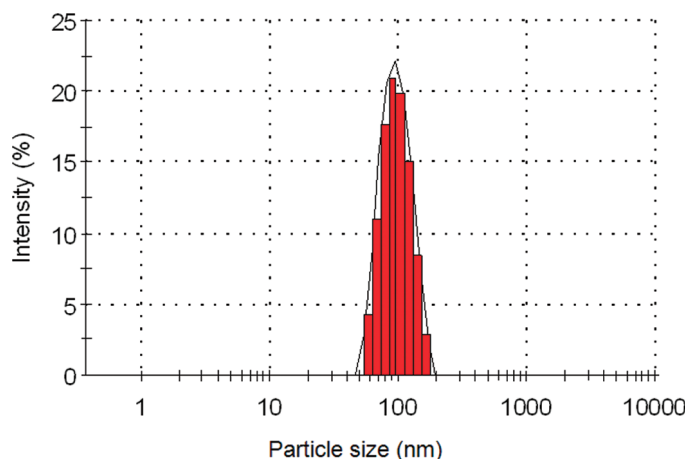


Figure 1. Size distribution of $[^3\text{H}/^{14}\text{C}]$ -solid lipid nanoparticles.

anti-inflammatory agent DEX, the therapeutic ratio of several chemotherapeutic agents can be simultaneously improved due to the reduction of physiological barriers to their uptake in tumors.^{11–13} NPs were pegylated by substituting a portion of the surfactants in the formulation with a polyethylene glycol (PEG) lipid to secure the PEG coverage on the NP surface and reduce their clearance by the reticuloendothelial system.⁹ Increased retention in the circulation may augment the passive accumulation of nanoparticles in tumors through the enhanced permeability and retention (EPR) effect.^{14,15} The palmitate ester of DEX (DEX-P) was encapsulated in the NPs, which are expected to release DEX in tumors by an enzymatic triggering mechanism.^{10,16} High esterase activity in tumor tissues will dramatically increase the conversion rate of DEX-P to DEX and release the drug from NPs, but DEX-P will remain intact in human plasma due to its low esterase activity.^{10,17} To achieve this design, the stability of drug encapsulation in NPs in the circulation is critical. The potency of the nanocarrier system largely depends on the properties of the individual nanoparticles. In this paper, we report on the uniformity of DEX-P payload in solid lipid nanoparticles as well as the stability of the drug–nanoparticle association in human plasma in or-

der to better predict the fate of the nanoparticles *in vivo*.

RESULTS AND DISCUSSION

Preparation of $[^3\text{H}/^{14}\text{C}$ Dual-Labeled Nanoparticles. We have developed a process referred to as “nanotemplate engineering” as an inexpensive, reproducible, and scalable nanoparticle formation process that avoids many of the issues associated with the preparation of other nanocarrier systems.¹⁸ This technology is based on the entropy-driven and spontaneous formation of a microemulsion that can easily be used as a nanotemplate to form nanoparticles from the dispersed droplet phase. After solidification, nanoparticle suspensions are translucent with visible opalescence. The particle suspension of DEX-P NPs produced by nanotemplate engineering containing radiolabeled drug ($[^3\text{H}]\text{-DEX-P}$) and lipid ($[^{14}\text{C}]$ -stearyl alcohol (SA)) has a narrow size distribution (Figure 1). The mean particle size of the $[^3\text{H}/^{14}\text{C}]$ -NPs was 93.2 ± 0.5 nm. Ultrafiltration (UF) and gel filtration chromatography are widely used to separate free drugs and determine the encapsulation efficiency. After the UF, the particle size increased to 99.6 ± 0.8 nm due to repeated concentrations and dilutions. The membrane binding was demonstrated to be minimal on the basis of the recovery of the free drug from ultrafiltration (>98%). Only 2.1% and 2.7% of radioactivity from $[^3\text{H}]\text{-DEX-P}$ and $[^{14}\text{C}]$ -stearyl alcohol, respectively, was detected in the UF filtrates; thus the encapsulation efficiency was 97–98%.

Gel Filtration Chromatography of Dual-Labeled DEX-P Nanoparticles.

In a parallel experiment, the $[^3\text{H}/^{14}\text{C}]$ -NPs were passed through a GFC column packed with Sepharose CL-2B. Interestingly, the chromatogram yielded two distinct peaks containing ^3H (DEX-P) and one peak containing ^{14}C (SA) when PBS was the elution buffer (Figure 2A). In contrast, when the column was eluted with water, both DEX-P and SA were eluted in a single peak (Figure 2B). DEX-P is extremely lipophilic; its aqueous solubility was determined to be $1.57 \mu\text{g}/\text{mL}$ by the filtration method and $2.08 \mu\text{g}/\text{mL}$ according to the centrifugation method. The concentration of DEX-P

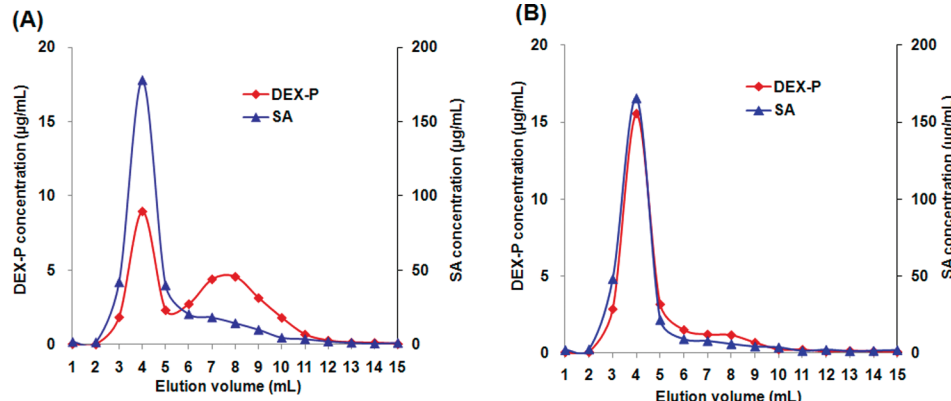


Figure 2. GFC profile of purified $[^3\text{H}/^{14}\text{C}]$ -NPs eluted by PBS (A) or water (B).

TABLE 1. Properties of the Original NP and the Fractions from GFC ($n = 3$)

	mean diameter (nm)	polydispersity index	zeta potential (mV)	DEX-P/SA (w/w)	recovery of DEX-P (%)	recovery of SA (%)
original NP	93.2 \pm 0.5	0.045 \pm 0.005	-8.9 ± 0.4 (water) -0.3 ± 0.1 (PBS)	0.10 \pm 0.05		
NP-peak 1 (PBS elution)	117.2 \pm 0.5	0.105 \pm 0.018	-1.3 ± 0.2	0.04 \pm 0.01	34.6 \pm 2.2	76.6 \pm 3.5
NP-peak 2 (PBS elution)	78.3 \pm 0.4	0.084 \pm 0.023	-3.3 ± 0.5	0.25 \pm 0.03	60.5 \pm 2.5	19.8 \pm 1.2
NP-peak (water elution)	95.8 \pm 0.6	0.115 \pm 0.006	-31.0 ± 2.1	0.08 \pm 0.01	94.3 \pm 2.1	93.9 \pm 2.3

in the later fractions was greater than the solubility of DEX-P, suggesting that the second peak was not comprised of free DEX-P. The recovery of radioactivity from the GFC process was greater than 98%.

According to the GFC profile (Figure 2A), fractions 3–5 (peak 1; elution volume = 3–5 mL) are distinguished from fractions 6–10 (peak 2; elution volume = 6–10 mL). The properties of the original NPs and the particles observed in the different GFC fractions are summarized in Table 1. It is notable that the particles recovered in peak 1 had a larger mean particle size than the particles recovered in peak 2, but both are greater than the exclusion limit of the Sepharose CL-2B, *i.e.*, 70–40 000 kD. On the basis of the equation $R = 0.051 \times M_w^{0.378}$, the pore size of the gel was calculated to be 7–76 nm in diameter.¹⁹ The prepared nanoparticles before GFC had a size distribution ranging from 50 to 190 nm (Figure 1). If size exclusion is the only mechanism governing the retention on the column, then small particles will enter the pores and be separated from the particles larger than 76 nm. However, retention on gel filtration chromatography columns can also be influenced by ion exclusion (electrostatic repulsion), adsorption, or other secondary effects.²⁰ Sepharose CL-2B is a bead-formed gel prepared from 2% cross-linked agarose. The gel possesses a small number of negatively charged groups and has some lipophilic character. The zeta potential of the prepared NPs in water was -8.9 ± 0.4 mV. The negative charge may result in electrostatic repulsions that prevent the NPs from entering the pore. Thus, all particles were eluted together near the exclusion limit in water.⁹ After chromatography, the zeta potential of NPs decreased to -31.0 ± 2.1 mV although they were still in water. A possible reason was that the gel interacted with the NPs and altered the surface properties of NPs. Caution should be applied when gel filtration chromatography is used to purify nanoparticles using a mobile phase containing no or low salt concentration. It is likely that the increased salt concentration reduced the charge effect of the NPs. The zeta potential of the NPs in PBS was close to neutral. Electrostatic repulsion is diminished, and size-based fractionation and gel adsorption became the dominant factors in the chromatography of the NPs.²¹ The particles recovered from peak 2 had a mean size close to the exclusion limit of 76 nm but were retained on the column longer and were separated from peak 1, possibly due to interaction with the gel. High salt concentration can

enhance the lipophilicity of the gel and lead to a stronger hydrophobic interaction with the particles. No significant differences were observed in the GFC profiles when Sepharose CL-4B or Sepharose 4B (separation range 60–20 000 kD) was used in place of Sepharose CL-2B. Two NP distributions consistently appeared when PBS was used as the elution buffer (data not shown). In addition, elution of the NPs with other mobile phases (10 and 100 mM phosphate buffers containing 0, 50, 155, or 300 mM NaCl, saline, 10 and 100 mM Tris-HCl buffer, and 100 mM HEPES buffer) resulted in similar GFC profiles (data not shown).

The particles recovered from peak 1 and peak 2 exhibited different properties, indicating that two different NP populations were present in the original NP suspension. The first population was comprised of larger particles with a greater lipid content (average drug/lipid ratio = 0.04), while the second population contained smaller particles encapsulating more DEX-P (average drug/lipid ratio = 0.25). When [³H]-DEX-P solution was loaded onto the column, the elution volume was 10 mL and the chromatogram did not overlap with the second population of the NP chromatogram. When Sephadex G-100 (separation range 4–150 kD) was used instead of Sepharose CL-2B, only one peak right at the void volume was obtained (figure not shown). These results proved that the particles recovered from both peak 1 and peak 2 have sizes of >150 kD (~ 9 nm). To ensure that the two NP populations were not generated by the GFC column, samples from peak 1 and peak 2 were reloaded onto the Sepharose CL-2B column; GFC profiles were the same as their initial elution (Figure 3). These studies all point to the existence of two distinct NP populations in the prepared NP suspension. As illustrated in Figure 3, the first population may be composed of a large amount of lipid mixing with DEX-P. On the basis of the previously reported rapid cleavage of NP-loaded DEX-P to DEX, the DEX-P molecules were expected to align in the microemulsion precursor with the DEX group directed toward the aqueous phase and the hydrophobic palmitate chain embedded in the oil phase.¹⁰ The NPs were stabilized by the surface coverage of surfactants. When DEX-P was mixed with a lower amount of lipid, DEX-P may have been oriented between the lipid and the surfactants. The DEX group is less lipophilic than the lipid (SA), and it may replace a portion of the surfactants to stabilize the NP surface. As a consequence, the surface of the second population

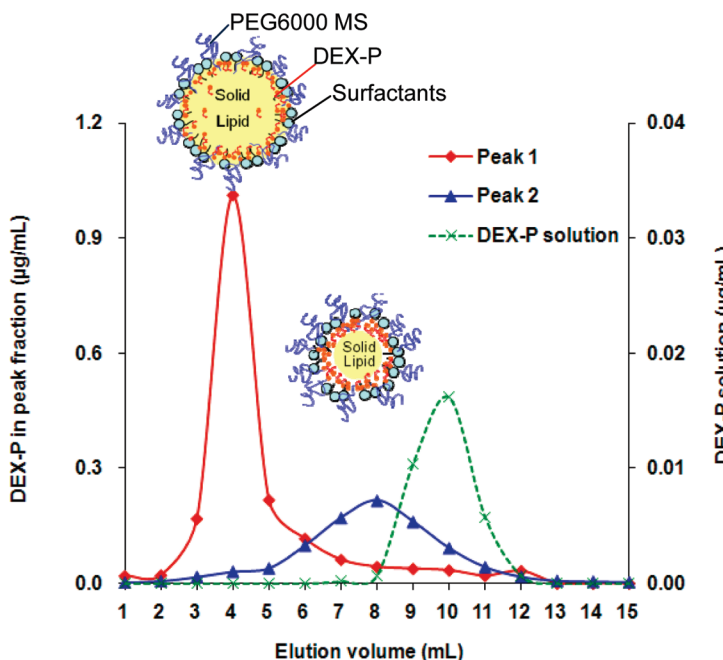


Figure 3. GFC profile of peak 1 and peak 2 reloaded onto the Sepharose CL-2B column using PBS as elution buffer.

can be more lipophilic compared with the first population. It may also be possible that DEX-P prefers an interface with higher curvature, resulting in a higher drug/lipid ratio in the second NP population.

Interaction of Nanoparticles with Human Serum Albumin.

The stability of nanoparticles and the retention of the therapeutic agent in the NPs while in the circulation is a critical factor, especially in light of the fact that there appear to be two populations of particles in the NP suspension. The physiological environment in plasma is complex. Opsonin proteins in plasma may adsorb onto the NPs and stimulate phagocytosis, thus affecting the particle biodistribution, biocompatibility, and therapeutic efficacy.^{22,23} These blood proteins come into contact with nanoparticles typically by random Brownian motion. Once sufficiently close to the surface of a particle, attractive forces such as van der Waals, electro-

static, ionic, hydrophobic/hydrophilic, and others can be involved in the binding of proteins to the surface of nanoparticles.²³ The interaction of proteins with NPs may also affect the integrity of the NPs. In order to simplify the study of NP stability in plasma, a NP suspension was added to solutions of human serum albumin (HSA), the most abundant protein in plasma. HSA concentrations were determined using the BCA assay, and it was confirmed that NPs did not cause interference with this assay at low NP concentration (>5 times dilution of the original NP suspension). The GFC elution profile of the mixture of NPs and HSA on the Sepharose CL-2B column is shown in Figure 4.

After mixing the HSA solution with the NP suspension, the HSA elution profile appeared to overlap with [³H]-DEX-P and [¹⁴C]-SA chromatograms when the sample was eluted with water. The shift of the HSA elution profile after mixing with NPs indicated that the protein may interact with the NPs in water. However, when eluting the column with PBS, HSA was completely separated from the first DEX-P NP population and eluted immediately after the second population. Apparently no protein adsorption occurred with the first NP population, but, due to the lack of separation between HSA, the NP-HSA complex, and the second NP population, it was unclear if HSA remained free in solution or if it was bound to the second NP population. High-performance liquid chromatography (HPLC) was used to elucidate this using a TSK-GEL G3000 SW column, chosen because of its separation range of 10–500 kD. We expected that nanoparticles would be eluted in the void volume, but the retention time of HSA would be greater. HSA was eluted at 15.5 min (dimer) and 17.5 min (monomer), while the NPs had a retention time of only 11.2 min as indicated by DEX-P (Figure 5). Only one NP peak was observed with this column separation. Immediately following the mixing of HSA and NPs, the

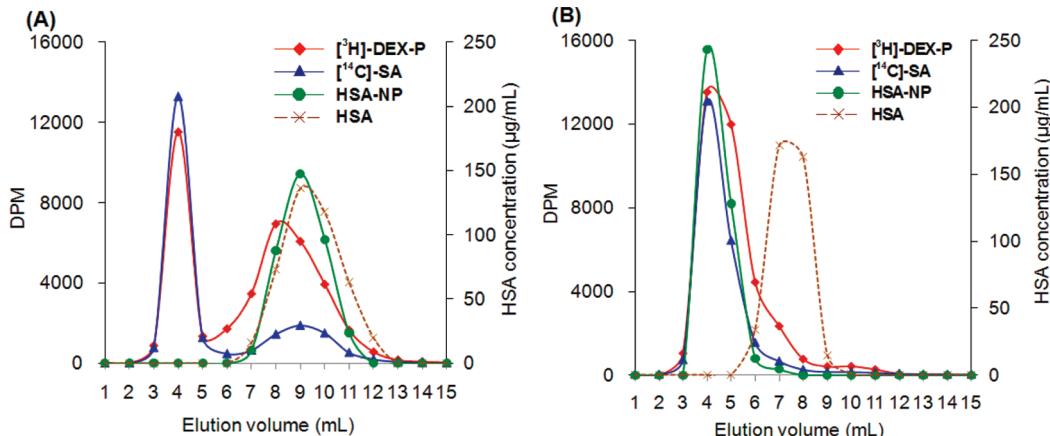


Figure 4. Sepharose CL-2B GFC profile of HSA and NP mixture with PBS (A) and water (B) elutions. The radioactivity of [³H]-DEX-P and [¹⁴C]-SA was plotted in terms of disintegrations per minute (DPM). The concentrations of HSA alone and in the NP suspension were determined by the BCA assay.

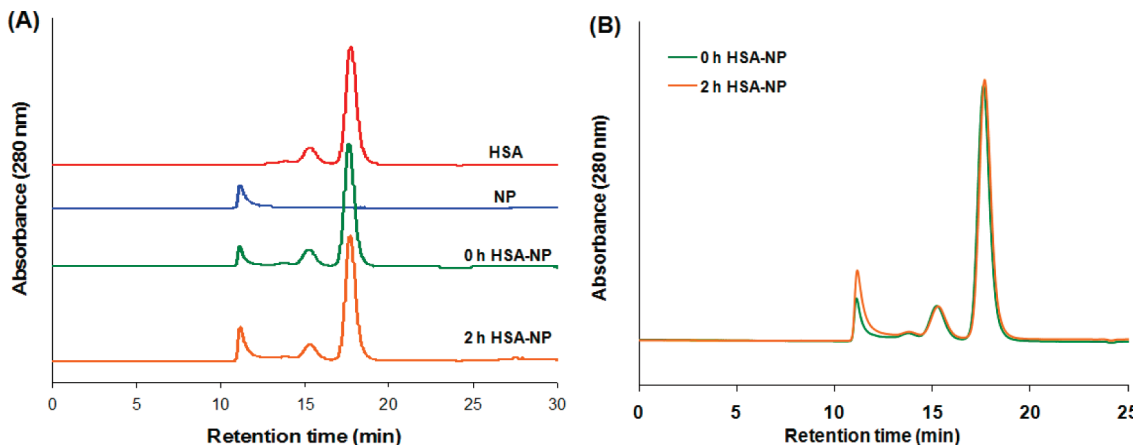


Figure 5. Gel filtration-HPLC profile of HSA and NP mixture before and after a 2 h incubation at 37 °C. It was conducted on a TSK G3000 SW column at 280 nm. The mobile phase was 0.1 M phosphate buffer containing 0.1 M Na_2SO_4 , pH 6.7, and the flow rate was 0.5 mL/min.

HPLC profile of each component in the mixture showed no significant difference from the individual HPLC curves (Figure 5A). After a 2 h incubation, the NP peak area was statistically different from that observed before incubation (Figure 5B). On the basis of the absorbance scan from 200 to 800 nm, the maximum absorbance for the NPs shifted from 240 to 245 nm, demonstrating the effect of protein adsorption. However, the amount of HSA associated with NPs was so low that no HSA loss was identified on the basis of the free HSA concentration. The results of both the gel filtration-HPLC (Figure 5) and GFC studies (Figure 4A) indicated that there may have been a slight amount of HSA adsorbed onto the second population of NPs but that no protein was bound to the first NP population. This may be due to a slight increase in the lipophilicity of the surface of the second population.

Stability of Nanoparticles in Human Plasma. Although there appear to be two particle populations with different drug and lipid content, in the presence of HSA, only minimal protein adsorption was observed. The majority of drug may be expected to remain associated with NPs. Our previous study on the *in vitro* release of DEX-P from solid lipid NPs demonstrated that <4% of DEX-P was detected in the UF filtrate when the NPs were incubated in PBS or human plasma at 37 °C for 24 h.¹⁰ Conversely, the release of DEX-P from NPs when incubated in mouse plasma was very rapid due to its high esterase activity, resulting in the cleavage of DEX-P to the less lipophilic DEX.¹⁰ However, we could not conclude that the NPs were intact and that the DEX-P remained associated with the NPs after a 24 h incubation in plasma. The possibility exists that the drug was initially stripped from the NPs by serum proteins. If this was the case, in plasma with low esterase activity (e.g., human plasma), the DEX-P would be recovered in the retentate following ultrafiltration due to the formation of drug aggregates or a drug–protein complex. Thus, it would not be possible to distinguish between radiolabeled DEX-P associated with NPs and protein-bound

DEX-P, as there is no reliable method to separate nanoparticles from plasma protein. The nanoparticles we produced have an average density of 1.05 g/cm³. Centrifugation at 40000g for 4 h cannot completely sediment the NPs. Use of GFC as a separation method is affected by the complexity of plasma, including its salt and metal components, and may produce confounding results. Thus, we developed a stepwise filtration method to evaluate the stability of drug association with NPs in human plasma. We hypothesized that nanoparticle-encapsulated DEX-P will exist in three forms after incubation with human plasma: (1) DEX-P encapsulated in NPs, (2) DEX-P solubilized in plasma (including protein-bound DEX-P), and (3) drug aggregates (unsolubilized drug). The encapsulated DEX-P and the solubilized DEX-P will both pass through a 0.2 μm filter, while drug aggregates would not be expected to pass through the filter. Protein-bound drug can be separated from free drug using ultrafiltration (MWCO 10 kD). The concentration of DEX-P in the filtrate represents free (unbound) DEX-P. The ratio of bound to unbound drug is constant when protein concentration is much greater than drug concentration. It is assumed that the stearyl alcohol component of the nanoparticles would exist in the same three forms as DEX-P.

When DEX-P and SA solubilized in PBS were subjected to ultrafiltration, their recoveries were ~98%. Both DEX-P and SA were observed to be highly protein bound (64% and 90%, respectively) under the conditions of this experiment. The amounts of DEX-P and SA associated with the NPs in a pilot study were above 82%. After incubating the NPs with human plasma at 37 °C for 24 h, <8% of the DEX-P or SA formed aggregates that were not able to pass through a 0.2 μm filter and ~10% of the solutes were released from the NPs. DEX-P and SA were consistent in terms of the percentage of aggregates and release.

The two NP populations were compared in terms of the recovery of DEX-P from microfiltration (0.2 μm), release of DEX-P from NPs, and association of DEX-P

TABLE 2. Association of DEX-P with NPs during a 24 h Incubation in PBS or 50% Human Plasma

sample	incubation time (h)	unaggregated DEX-P (%) ^a	released DEX-P (%) ^b	NP-associated DEX-P (%) ^c
NP in PBS	0	98.4 ± 0.5	0.8 ± 0.5	97.6 ± 0.6
	2	97.8 ± 1.4	1.2 ± 0.2	96.6 ± 1.3
	24	97.8 ± 1.5	1.6 ± 0.1	96.2 ± 1.6
NP in plasma	0	98.1 ± 2.3	3.0 ± 0.2	95.2 ± 2.2
	2	98.1 ± 3.0	4.2 ± 0.5	93.9 ± 2.7
	24	93.2 ± 1.2	7.7 ± 0.6	85.5 ± 1.8 ^d
NP-peak 1 in plasma	0	97.8 ± 2.0	1.4 ± 1.2	96.4 ± 3.2
	2	98.0 ± 2.2	2.4 ± 1.9	95.5 ± 3.8
	24	96.6 ± 1.8	3.5 ± 1.5	93.0 ± 1.1
NP-peak 2 in plasma	0	97.4 ± 4.2	1.6 ± 0.7	95.8 ± 3.9
	2	99.2 ± 0.3	5.2 ± 1.0	94.1 ± 0.7
	24	88.1 ± 3.5	8.7 ± 1.6	79.4 ± 1.9 ^d

^aCalculated from the recovery of DEX-P after microfiltration using a 0.2 μ m syringe filter. ^bCalculated from the percentage of DEX-P in the filtrate of ultrafiltration (MWCO: 10 kD) and corrected based on 98% membrane recovery (in PBS) and 64% protein binding (in plasma). ^cCalculated from the following equation, NP-associated DEX-P (%) = *a* - *b*. ^dSignificantly different from 0 and 2 h time points of this sample.

with NPs during the 24 h incubation in PBS or 50% human plasma (Table 2). The results reveal that, after a 24 h incubation in PBS, greater than 96% of DEX-P was associated with NPs, while after incubation of the NPs in human plasma, more DEX-P aggregates formed and a greater percentage of the drug was released from the NPs. According to the ANOVA one-way test, there was no significant difference between NPs in PBS and NP-peak 1 in plasma within the 24 h incubation. For NPs in plasma and NP-peak 2 in plasma groups, the difference in NP-associated DEX-P between 0 and 2 h incubation was not significant, but the aggregates and amount of DEX-P released increased and the NP-drug association was significantly different at the 24 h time point ($P < 0.05$). The NP-associated DEX-P was significantly different among the four groups after a 24 h incubation ($P < 0.05$). NPs isolated from peak 1 showed better stability than NPs isolated from peak 2; however, in both populations, DEX-P was predominantly associated with the NPs in the challenging plasma environment.

Particles with a diameter of approximately 90 nm were observed by TEM after incubating NPs in PBS and human plasma at 37 °C for 24 h (Figure 6). These TEM images supported the stability data and indicated that most particles remained intact in human plasma after a 24 h incubation. The dark background in the image of the NPs in human plasma results from the presence of plasma proteins and other components.

CONCLUSION

Drug encapsulation in nanocarrier systems is generally characterized in terms of an entire population of nanoparticles, assuming that drug distribution is uniform and the NP population is homogeneous. In this study in which solid lipid nanoparticles were prepared containing labeled drug ($[^3\text{H}]\text{-DEX-P}$) and lipid ($[^{14}\text{C}]\text{-steraryl alcohol}$), two NP populations were revealed from a GFC separation using Sepharose CL-2B. The drug appeared to be deposited differently in the two NP populations. The first population contained larger particles with an average drug/lipid ratio of 0.04, and the second contained smaller particles with an average drug/lipid ratio of 0.25. The GFC and HPLC profiles of the mixture of NPs and HSA solution proved that the first population had no HSA adsorption, but there may have been a slight amount of HSA adsorbed onto the second population of NPs. After incubation in 50% human plasma at 37 °C for 24 h, >80% of DEX-P appeared to be associated with NPs. The first population of NPs showed better stability in human plasma, but both populations demonstrated relatively strong drug-NP association against the harsh plasma environment. The second population of NPs contains higher drug content and, thus, is more desirable from a payload delivery perspective. Characterization of these nanoparticles may be challenging from a regulatory perspective, but the strong association of DEX-P with the NPs in plasma indicated that this nanocarrier system has the potential to deliver a prodrug DEX-P to tumors and to release the chemotherapy adjuvant DEX in a bioresponsive manner in order to enhance the effectiveness of subse-

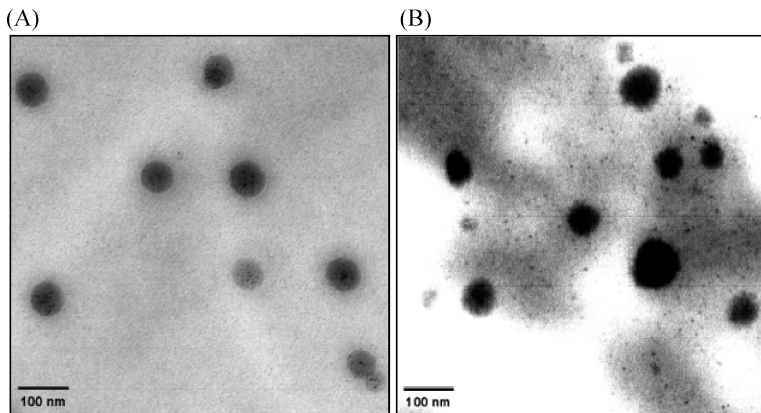


Figure 6. TEM of NPs in PBS (A) and human plasma (B) after 24 h incubation at 37 °C.

quently administered chemotherapeutic agents. *In vivo* studies will determine if there is a therapeutic differ-

ence between these NP populations and will serve as a guide when designing future nanocarrier systems.

MATERIALS AND METHODS

Materials. Tritiated dexamethasone [6,7-³H(N)] (specific activity = 35–50 Ci/mmol) and [¹⁴C]-stearyl alcohol (octadecanol [1-¹⁴C]; specific activity = 50–60 mCi/mmol) were purchased from American Radiolabeled Chemicals Inc. (Saint Louis, MO, USA). Stearyl alcohol, polysorbate 60, and Brij78 were obtained from Uniqema (Chicago, IL, USA). PEG6000 monostearate (PEG6000 MS) was a gift from Stepan (Northfield, IL, USA). Centrifugal filter devices (Microcon YM-10 and Microcon YM-50) were purchased from Millipore (Bedford, MA, USA). Sepharose CL-2B and Sephadex G-100 were purchased from GE Healthcare (Piscataway, NJ, USA). Human plasma containing sodium heparin as the anticoagulant was purchased from Innovative Research, Inc. (Novi, MI, USA). The BCA protein assay kit was purchased from Thermo Fisher Scientific Inc. (Rockford, IL). Liquid scintillation cocktail Optiphase HSafe 3 was purchased from PerkinElmer (Waltham, MA, USA).

Preparation of ³H/¹⁴C Dual-Labeled Nanoparticles. All NPs were prepared using the “nanotemplate engineering” technique. The procedures to prepare radiolabeled DEX-P NPs have been previously described.^{2,3} Briefly, [³H]-DEX-P was synthesized by the reaction of [³H]-DEX and palmitoyl chloride. Nanoparticles were derived from a microemulsion comprised of ¹⁴C-stearyl alcohol and nonlabeled stearyl alcohol (2 mg/mL), [³H]-DEX-P and nonlabeled DEX-P mixture (0.2 mg/mL), polysorbate 60 (0.5 mg/mL), Brij78 (3.5 mg/mL), and PEG6000MS (3.5 mg/mL). Addition of warm DI water (pH 7.4, 70 °C) to the melted mixture of lipid, drug, and surfactants yielded a microemulsion. After stirring in a 70 °C water bath for 1 h, the warm microemulsion was cooled to 25 °C, resulting in the formation of nanoparticles. Particle size distribution and zeta potential were measured in triplicate by photon correlation spectroscopy using a Zetasizer Nano ZS (Malvern, Worcestershire, UK). The nanoparticle suspension was purified using a 0.2 μm filter to remove large particles and using an ultrafiltration filter (MWCO 50 kD) to remove free surfactants and drug. The retentate was washed four times and resuspended in DI water. Solubilized [³H]-DEX-P and [¹⁴C]-stearyl alcohol obtained from the UF filtrate were refiltered using a new UF filter to determine the membrane binding. The radioactive content of the nanoparticle suspension was quantified by mixing the NP suspension with 5 mL of liquid scintillation cocktail and counting using a Tri-Carb liquid scintillation counter (LSC; PerkinElmer). The corrected specific activity of [³H]-DEX-P and [¹⁴C]-stearyl alcohol was calculated by dividing radioactivity by total mass.

Gel Filtration Chromatography of Dual-Labeled DEX-P Nanoparticles. Gel filtration chromatography was performed by using a column (10 × 1.0 cm) packed with Sepharose CL-2B, Sepharose CL-4B, Sepharose 4B, or Sephadex G-100. The bed volume was 8 mL. Two hundred microliters of prepared [³H/¹⁴C]-NPs were applied to a pre-equilibrated column and eluted with either DI water or 5 mM sodium phosphate buffer (PBS, containing 0.155 mM NaCl, pH 7.4) at a flow rate of 30 mL/h. Fractions (1 mL) were collected, and radioactivity in 100 μL aliquots was counted. The particle size and zeta potential of the fractions were determined in the same way as described above. To confirm that the chromatography process did not alter the NPs or create new peaks, the peak fractions were reloaded onto the column and eluted with PBS. [³H]-DEX-P was applied to the column and eluted with PBS to locate the free drug peak. Similar procedures were used in the elution of NPs with other mobile phases (pH 7.4), including 10 and 100 mM phosphate buffers containing 0, 50, 155, or 300 mM NaCl, saline, 10 and 100 mM Tris-HCl buffers, and 100 mM HEPES buffer. The mass of DEX-P and SA in each fraction was calculated by dividing the amount of radioactivity in the fraction by the corrected specific activity. Drug/lipid ratios were determined by the mass ratios of DEX-P to SA.

The solubility of DEX-P in PBS was determined by dissolving a mixture of DEX-P (0.5 mg) and [³H]-DEX-P (8.4 μg, 0.94 μCi) in

chloroform. The chloroform was evaporated in a 75 °C water bath, and 2 mL of PBS was added following by vortexing of the mixture. The suspensions were subsequently incubated at room temperature for 24 h. Three hundred microliters of the DEX-P suspensions were centrifuged at 20000g for 60 min. The remainder of the suspensions was passed through two 0.2 μm sterile filters in sequence, and the amount of radioactivity in 100 μL aliquots of each filtrate was quantified by liquid scintillation counting. The second filtration demonstrated that the membrane binding was less than 2%. The solubility of DEX-P in PBS was determined on the basis of the measured radioactivity in the filtrates or supernatant.

Interaction of Nanoparticles with Human Serum Albumin. Two hundred microliters of an aqueous HSA solution (10 mg/mL) was mixed with 200 μL of [¹⁴C/³H]-NPs and incubated at 37 °C for 2 h. After incubation, 100 μL of the mixture was loaded onto a Sepharose CL-2B column and eluted with water or PBS. Fractions (1 mL) were collected, and the protein concentration in each fraction was determined using the BCA assay. The radioactivity in each sample was quantified by liquid scintillation counting. In order to rule out the interference of NPs in the BCA assay, a solution of HSA of a known concentration (500 μg/mL) was mixed with various dilutions of NP suspensions, and protein concentration was measured using the BCA assay.

In order to achieve baseline separation of NPs from HSA, a Shimadzu Prominence Ultra Fast Liquid Chromatography (UFLC) system equipped with a gel filtration-HPLC column, TSK-GEL G 3000 SW (7.5 mm i.d. × 30 cm), and a diode array detector was used. The mobile phase was 0.1 M Na₂SO₄ in 0.1 M phosphate buffer, pH 6.7. DEX-P NPs containing no radiolabels were prepared using the same method as radiolabeled NPs but without the addition of radiolabeled DEX-P and SA. NPs and HSA solution (10 mg/mL) were mixed at 1:1 (v/v) ratio and incubated at 37 °C for 2 h. The mixture at time 0 and 2 h, 2× diluted HSA solution in PBS (5 mg/mL), and 2× diluted NPs in PBS were injected onto the HPLC column with an injection volume of 20 μL. The elution was monitored at wavelengths of 240 nm for DEX-P and 280 nm for HSA.

Stability in Human Plasma. To determine the protein binding ratio in human plasma, radiolabeled DEX-P and SA solutions in human plasma were prepared by mixing DEX-P (0.5 mg)/[³H]-DEX-P and SA (0.5 mg)/[¹⁴C]-SA with 2 mL of human plasma. The mixtures were filtered through a 0.2 μm sterile filter, and 100 μL of each filtrate was measured for radioactivity. Three hundred microliters of each filtrate was centrifuged at 8000g for 30 min in an ultrafiltration tube (MWCO 10 kD) in duplicate, and 50 μL of the UF filtrates were measured for radioactivity. Two hundred microliters of the UF filtrates were again centrifuged at 8000g for 30 min in an ultrafiltration tube (MWCO 10 kD), and 100 μL of each UF filtrate was measured for radioactivity. The binding of the solute to the UF membrane was determined on the basis of the loss of radioactivity in the filtrate before and after the second ultrafiltration. The recovery from the filtrations and the percentage of free drug in human plasma were calculated accordingly and recorded as membrane recovery and protein unbound ratio, respectively.

To mimic the *in vivo* condition, 50% human plasma was used to study the NP stability. [³H/¹⁴C]-NP suspensions were mixed with PBS or 50% human plasma (1:14, v/v) in a final volume of 1.5 mL and then filtered through a 0.2 μm filter. The filtrates were incubated at 37 °C for 24 h, followed by filtration through a 0.2 μm filter. The loss of radioactivity after the filtration (0.2 μm) was assumed to be due to the precipitation of aggregates. Two hundred microliters of the filtrates was centrifuged at 8000g for 30 min in an ultrafiltration tube (MWCO 10 kD), and 100 μL of the UF filtrates were measured for radioactivity. The NP suspension and NP peak 1 and peak 2 fractions (elution volume = 4 and 8 mL, respectively) were mixed with 50% human plasma and incubated at 37 °C for 24 h. The percent of

the DEX-P or SA associated with NPs (% NP associated) was calculated using the equation

$$\% \text{ NP associated} = \frac{\% \text{ in filtrate (0.2}\mu\text{m filter}) - \% \text{ in filtrate (10 kD filter)}}{\text{protein unbound ratio}}$$

Transmission electron microscopic (TEM) images (85 000 \times magnification) of the mixture of NPs in PBS or human plasma were obtained after a 24 h incubation. A drop of the NP/plasma suspension was deposited on a copper mesh carbon-coated grid and allowed to settle for 2 min at room temperature. After removal of excess fluid, the grid was air-dried for 2 h before obtaining the TEM image (ZEISS EM900, Jena, Germany).

Statistical Analysis. Data are presented as mean \pm standard deviation ($n = 3$). Groups were compared using analysis of variance (ANOVA) one-way test with SigmaStat 3.5 software (Systat Inc., San Jose, CA). Differences were considered statistically significant when $P < 0.05$, and the Holm–Sidak method was used to perform pairwise multiple comparisons on significant effects and interactions.

Acknowledgment. The authors are grateful for financial support from the Benedict Cassen Postdoctoral Fellowship from the Education and Research Foundation for the Society of Nuclear Medicine (X.L.), the Carolina Partnership, and grant DGE-0653710 from the NSF IGERT Program (M.D.H.).

Supporting Information Available: Structures of the NP components and the HLB values of the surfactants. This material is available free of charge via the Internet at <http://pubs.acs.org>.

REFERENCES AND NOTES

- Meng, H.; Liang, M.; Xia, T.; Li, Z.; Ji, Z.; Zink, J. I.; Nel, A. E. Engineered Design of Mesoporous Silica Nanoparticles to Deliver Doxorubicin and P-glycoprotein siRNA to Overcome Drug Resistance in a Cancer Cell Line. *ACS Nano* **2010**, *4*, 4539–4550.
- Tang, Y.; Lei, T.; Manchanda, R.; Nagesetti, A.; Fernandez-Fernandez, A.; Srinivasan, S.; McGoron, A. J. Simultaneous Delivery of Chemotherapeutic and Thermal-Optical Agents to Cancer Cells by a Polymeric (PLGA) Nanocarrier: An In Vitro Study. *Pharm. Res.* **2010**, *27*, 2242–2253.
- Heidel, J. D.; Davis, M. E. Clinical Developments in Nanotechnology for Cancer Therapy. *Pharm. Res.* **2010**, DOI 10.1007/s11095-010-0178-7.
- Gil, P. R.; Parak, W. J. Composite Nanoparticles Take Aim at Cancer. *ACS Nano* **2008**, *2*, 2200–2205.
- Li, S. D.; Huang, L. Pharmacokinetics and Biodistribution of Nanoparticles. *Mol. Pharm.* **2008**, *5*, 496–504.
- Farrell, D.; Ptak, K.; Panaro, N. J.; Grodzinski, P. Nanotechnology-Based Cancer Therapeutics—Promise and Challenge—Lessons Learned Through the NCI Alliance for Nanotechnology in Cancer. *Pharm. Res.* **2010**, DOI 10.1007/s11095-010-0214-7.
- Brown, S. C.; Palazuelos, M.; Sharma, P.; Powers, K. W.; Roberts, S. M.; Grobmyer, S. R.; Moudgil, B. M. Nanoparticle Characterization for Cancer Nanotechnology and Other Biological Applications. *Methods Mol. Biol.* **2010**, *624*, 39–65.
- Hall, J. B.; Dobrovolskaia, M. A.; Patri, A. K.; McNeil, S. E. Characterization of Nanoparticles for Therapeutics. *Nanomedicine (London, U.K.)* **2007**, *2*, 789–803.
- Lu, X.; Howard, M. D.; Mazik, M.; Eldridge, J.; Rinehart, J. J.; Jay, M.; Leggas, M. Nanoparticles Containing Anti-Inflammatory Agents as Chemotherapy Adjuvants: Optimization and Characterization. *AAPS J.* **2008**, *10*, 133–140.
- Lu, X.; Howard, M. D.; Talbert, D. R.; Rinehart, J. J.; Jay, M.; Leggas, M. Nanoparticles Containing Anti-Inflammatory Agents as Chemotherapy Adjuvants II: Role of Plasma Esterases in Drug Release. *AAPS J.* **2009**, *11*, 120–122.
- Wang, H.; Li, M.; Rinehart, J. J.; Zhang, R. Pretreatment with Dexamethasone Increases Antitumor Activity of Carboplatin and Gemcitabine in Mice Bearing Human Cancer Xenografts: In Vivo Activity, Pharmacokinetics, and Clinical Implications for Cancer Chemotherapy. *Clin. Cancer Res.* **2004**, *10*, 1633–1644.
- Wang, H.; Li, M.; Rinehart, J. J.; Zhang, R. Dexamethasone as a Chemoprotectant in Cancer Chemotherapy: Hematoprotective Effects and Altered Pharmacokinetics and Tissue Distribution of Carboplatin and Gemcitabine. *Cancer Chemother. Pharmacol.* **2004**, *53*, 459–467.
- Leggas, M.; Kuo, K. L.; Robert, F.; Cloud, G.; Deshazo, M.; Zhang, R.; Li, M.; Wang, H.; Davidson, S.; Rinehart, J. Intensive Anti-Inflammatory Therapy with Dexamethasone in Patients with Non-Small Cell Lung Cancer: Effect on Chemotherapy Toxicity and Efficacy. *Cancer Chemother. Pharmacol.* **2009**, *63*, 731–743.
- Maeda, H. Tumor-Selective Delivery of Macromolecular Drugs via the EPR Effect: Background and Future Prospects. *Bioconjugate Chem.* **2010**, *21*, 797–802.
- Torchilin, V. P. Passive and Active Drug Targeting: Drug Delivery to Tumors as an Example. *Handb. Exp. Pharmacol.* **2010**, *197*, 3–53.
- Susan, L. P.; Roth, R. B.; Adkins, W. C. Regression of Prostatic Cancer Metastasis by High Doses of Diethylstilbestrol Diphasophate. *Urology* **1976**, *7*, 598–601.
- Liederer, B. M.; Borchardt, R. T. Enzymes Involved in the Bioconversion of Ester-Based Prodrugs. *J. Pharm. Sci.* **2006**, *95*, 1177–1195.
- Oyewumi, M. O.; Yokel, R. A.; Jay, M.; Coakley, T.; Mumper, R. J. Comparison of Cell Uptake, Biodistribution and Tumor Retention of Folate-Coated and PEG-Coated Gadolinium Nanoparticles in Tumor-Bearing Mice. *J. Controlled Release* **2004**, *95*, 613–626.
- Brissova, M.; Petro, M.; Lacik, I.; Powers, A. C.; Wang, T. Evaluation of Microcapsule Permeability via Inverse Size Exclusion Chromatography. *Anal. Biochem.* **1996**, *242*, 104–111.
- Mori, S. Secondary Effects in Aqueous Size Exclusion Chromatography of Sodium Poly(styrenesulfonate) Compounds. *Anal. Chem.* **1989**, *61*, 530–534.
- Haumaier, L.; Zech, W.; Franke, G. Gel Permeation Chromatography of Water-Soluble Organic Matter with Deionized Water as Eluent—I. Examination of the Method. *Org. Geochem.* **1990**, *15*, 413–417.
- Aggarwal, P.; Hall, J. B.; McLeland, C. B.; Dobrovolskaia, M. A.; McNeil, S. E. Nanoparticle Interaction with Plasma Proteins as It Relates to Particle Biodistribution, Biocompatibility and Therapeutic Efficacy. *Adv. Drug Delivery Rev.* **2009**, *61*, 428–437.
- Owens, D. E.; Peppas, N. A. Opsonization, Biodistribution, and Pharmacokinetics of Polymeric Nanoparticles. *Int. J. Pharm.* **2006**, *307*, 93–102.